Journal of Instrumentation

SISSA

The μ-RWELL for high rate application

Published by IOP Publishing for Sissa Medialab

Received: *May 14, 2020*
Accepted: *June 1, 2020*
Published: *September 9, 2020*

International Conference on Instrumentation for Colliding Beam Physics
Novosibirsk, Russia
24–28 February, 2020

The μ-RWELL for high rate application

G. Bencivenni,[a] **R. De Oliveira,**[b] **G. Felici,**[a] **M. Gatta,**[a] **M. Giovannetti,**[a,1] **G. Morello**[a] **and M. Poli Lener**[a]

[a] *Laboratori Nazionali di Frascati dell'INFN,*
Via E. Fermi 40, Frascati, Italy
[b] *CERN,*
Esplanade des Particules 1, Meyrin, Switzerland

E-mail: matteo.giovannetti@lnf.infn.it

Abstract: The micro-Resistive WELL (μ-RWELL) is a compact, simple and robust Micro-Pattern Gaseous Detector (MPGD) developed for large area HEP applications requiring the operation in harsh environment. The detector amplification stage, similar to a GEM foil, is realized with a polyimide structure micro-patterned with a blind-hole matrix, embedded through a thin Diamond-Like-Carbon (DLC) resistive layer with the readout PCB. The introduction of a resistive layer ($\rho = 50 \div 200\,\mathrm{M\Omega/\square}$) mitigating the transition from streamer to spark gives the possibility to achieve large gains ($> 10^4$), while affecting the detector performance in terms of rate capability. Different detector layouts have been studied: the most simple one based on a single-resistive layer, with edge grounding has been designed for low-rate applications (few tens of kHz/cm^2); more sophisticated schemes have been studied for high-rate purposes ($\geq 10\,\mathrm{MHz/cm^2}$). An overview of the different architectures studied for the high-rate version of the detector, together with their performance will be presented. The presence of the resistive layer also affects the charge spread on the strips and consequently the spatial resolution of the detector: a systematic study of the spatial resolution obtained with the charge centroid (CC) method as a function of the impinging angle was made. For non-orthogonal tracks the spatial resolution with CC method is compared with the performance obtained with the micro-TPC mode (μTPC): a readout approach that exploits the combined measurement of the ionization clusters time of arrival and the amplitude of the signals on the strips. Implementing the μTPC allows reaching an almost flat space resolution $< 100\,\mu m$ for a wide angular range. Finally the results of the detector aging campaign is presented, with detectors integrating up to 175 mC/cm^2 and bare DLC foils integrating a charge up to 800 mC/cm^2.

Keywords: Gaseous detectors; Micropattern gaseous detectors (MSGC, GEM, THGEM, RETHGEM, MHSP, MICROPIC, MICROMEGAS, InGrid, etc)

[1] Corresponding author.

https://doi.org/10.1088/1748-0221/15/09/C09034

2020 JINST 15 C09034

Contents

2020 JINST 15 C09034

1 Introduction

The μ-RWELL, figure 1, is a single-amplification stage resistive MPGD [1] that combines in a unique approach the solutions and improvements achieved in the last years in the MPGD field. The R&D has the purpose to improve the stability in heavy irradiated environment and simplifying the construction procedures in view of an easy technology transfer to industry.

The detector is composed of two elements: the cathode, a simple FR4 PCB with a thin copper layer on one side and the μ-RWELL_PCB, the core of the detector. The μ-RWELL_PCB, realized by means of standard photo-lithography technology, is composed of three different elements: a well matrix patterned polyimide (Apical®) foil[1] acting as amplification element of the detector; a resistive layer ($\rho = 50 \div 200\,\mathrm{M\Omega/\square}$) realized with a Diamond-Like-Carbon (DLC) film sputtered on the bottom side of the polyimide foil, as discharge limitation stage; a standard PCB, segmented as strip, pixel or pad electrodes, for readout purposes. Applying a suitable voltage between the copper layer and the DLC, the well acts as a multiplication channel for the ionization produced in the drift gas gap.

The spark suppression mechanism is similar to the one of the Resistive Plate Counters, [2, 3]: the streamer created inside the amplification volume, inducing a large current flowing through the resistive layer, generates a localized drop of the amplifying voltage with an effective quenching of the multiplication process in the gas. This mechanism suppressing the discharge amplitude allows to achieve large gains ($\geq 10^4$) with a single amplification stage. A drawback, correlated with the ohmic behaviour of the detector, is the reduced capability to stand high particle fluxes. A detector relying on this simple resistive layout suffers at high particle fluxes of a non-uniform response over its surface, that worsens as the size of the detector increases. This effect, correlated to the average resistance faced by the charge produced in the avalanche, actually depends on the distance between the particle incidence position and the detector grounding line.

[1] 50 μm thick polyimide covered on one side with 5 μm thick copper, similar to the GEM base material.

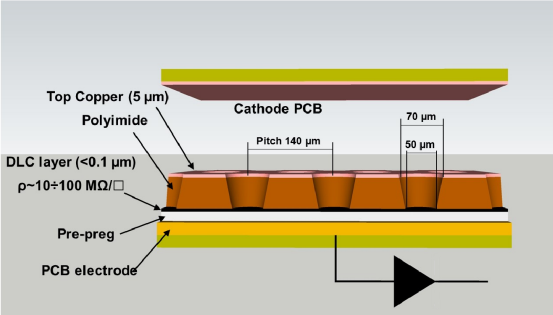

Figure 1. Layout of the µ-RWELL.

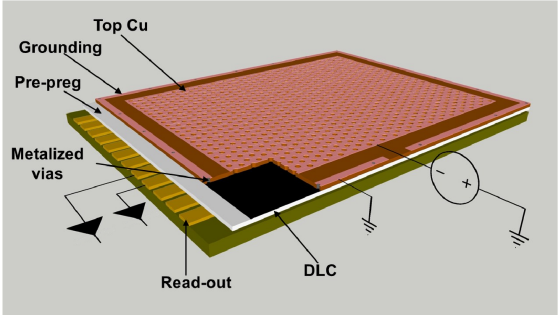

Figure 2. Sketch of the Single-Resistive layout.

The simplest scheme for the evacuation of the current in a µ-RWELL is based on a single resistive layer with a grounding line all around the active area, figure 2, (Single-Resisitive layout — SRL). For large area devices the path of the current to ground could therefore be large and strongly dependent on the incidence point of the particle.

In order to cope with this effect the solution is to reduce as much as possible the average path towards the ground connection, introducing a high density grounding network on the resistive stage. Two resistive layouts for high rate (HR) purposes have been built and extensively tested [4]: their performance in terms of efficiency and rate capability have been measured in different beam conditions at the CERN and PSI beam lines.

1.1 The High Rate layouts

The Silver-Grid (SG) layout, is sketched in figure 3. The conductive grid deposited on the DLC layer acts as a high density 2-D current evacuation system. The pitch of the grid together with the resistivity of the DLC are parameters of this layout. The presence of a conductive grid on the DLC can induce discharges over its surface requiring the introduction of a small dead zone in the amplification stage above the grid lines.

The Double-Resistive Layer (DRL) layout is sketched in figure 4. This layout aim to obtain a dense grounding network inside the active area without the need to introduce any dead zone (unlike the SG). The first DLC film, sputtered on the back-plane of the amplification stage, is connected to a second DLC layer by means of a matrix of metallized vias (v1). A further matrix of vias (v2) connects the second DLC film to the underlying readout electrodes, providing the final grounding of the whole resistive stage. The role of the second DLC layer is to ensure that the first set of vias (v1) is not connected direcly to ground, introducing an effective resistance between (v1) and (v2). The vias density is typically $\leq 1\,\mathrm{cm}^{-2}$. In this way a 3D-current evacuation layout is obtained.

1.2 Overall performance of the detectors

The µ-RWELL detectors were tested extensively during the last years [5, 6] always operating with $Ar/CO_2/CF_4$ (45/15/40) gas mixture. The relevant physical quantities are reported in this paper as a function of the detector gas gain to take into account small manufacturing differences in the amplification stage of the µ-RWELL prototypes (i.e. well diameter and shape). All the recent detectors produced can reach gain up to 10^4, figure 5. For the HR layouts, a rate capability up to $10\,\mathrm{MHz/cm}^2$ can be reached, with a detection efficiency of the order of $97 \div 98\%$, figure 6.

2020 JINST 15 C09034

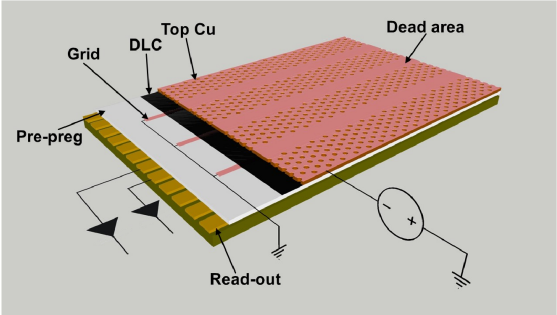

Figure 3. Sketchs for the SG layout.

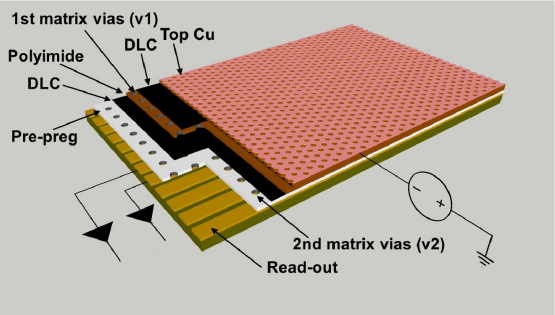

Figure 4. Sketchs for the DRL layout.

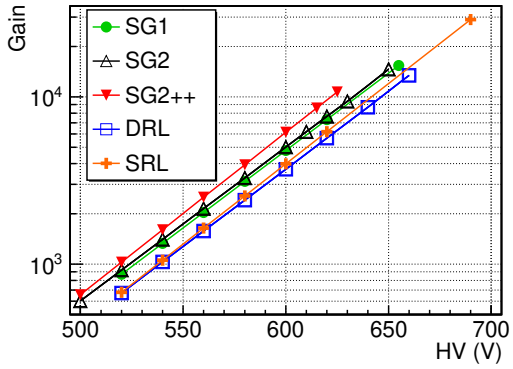

Figure 5. Gas gain calibration.

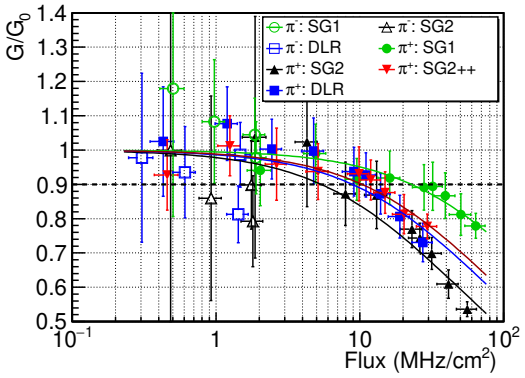

Figure 6. Rate capability measurements.

Table 1. The SG chambers show a higher efficiency thanks to an electron collection mechanism that reduces the effective dead zone.

Layout	DEAD AREA (mm)	Geometrical Acceptance	Max Efficiency	Δ%
DRL	0	100%	98%	
SG2++	0.6	95%	97%	2%
SG2	1.2	90%	93%	3%
SG1	2.0	66%	80%	14%

The mechanism behind the time resolution of a μ-RWELL is essentially the same of a GEM detector, depending on the position of the nearest ionization cluster produced in the gas [7] and the drift velocity of the gas mixture. The time resolution was measured using VFAT2-Asic Front End Electronics (FEE), achieving an asymptotic time resolution of 5.7 ns, figure 7, limited by the time resolution of the FEE.

In figure 8 the efficiency of the HR-layouts is reported as a function of the detectors gain. At a gain of 5000 the DRL shows an efficiency of 98%, while the SG1 and SG2 achieve a detection efficiency of 80% and 93% respectively, larger than their geometrical acceptance and the SG2++ tends to an almost full efficiency of about 97%, as summarized in table 1.

The efficiency larger than the geometrical acceptance of the SG prototypes was investigated.

2020 JINST 15 C09034

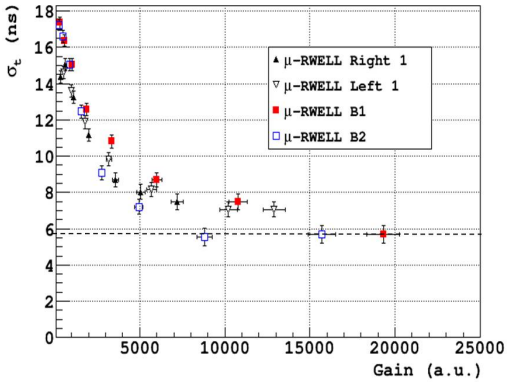

Figure 7. Time resolution for different prototypes.

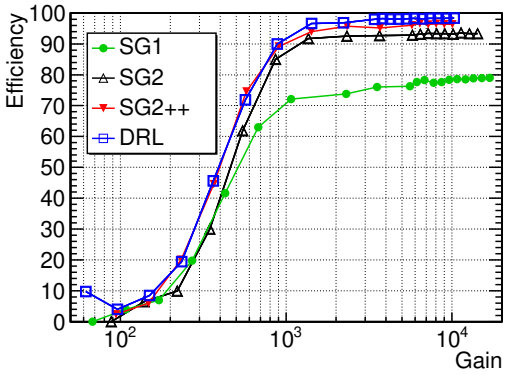

Figure 8. Efficiency as a function of the gas gain for the HR layouts

This effect is typical of detectors with GEM-like amplification stage [7, 8], and the efficiency and the charge profile for the SG1 are reported as example. In figure 9 (top) we plot the efficiency and in figure 9 (bottom) the charge as a function of the incidence point. The geometrical structure of the detector layout is visible on both: an efficiency drop and an increase of the charge are present in correspondence of the dead zones. Actually the wells close to the dead zones collect also the primary ionization produced above the inefficient regions ("focusing effect") resulting in a recovery of the detection efficiency; at the same time the amplification in these wells is increased probably due to the squeezing of the drift field lines. Moreover, as shown in figure 10, increasing the HV applied to the amplification stage the efficiency in the dead zone improves, as observed in GEM detectors (KLOE-2 CGEM [9]).

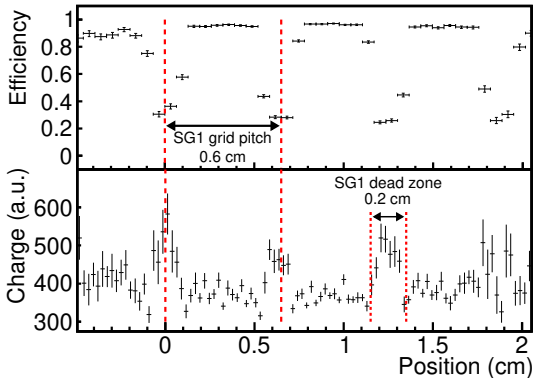

Figure 9. Efficiency and charge profile for the SG1 layout. The effects of the 2 mm wide dead zones and the 6 mm grid pitch are both visible.

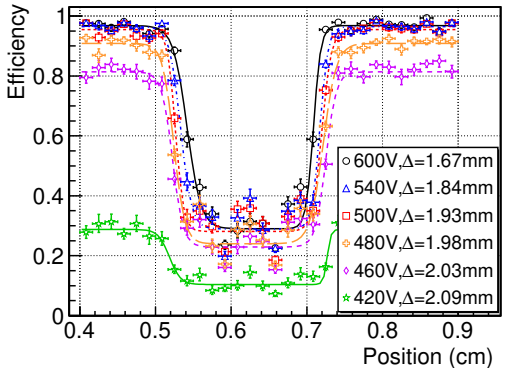

Figure 10. Zoom of the efficiency profile in the dead zone for different voltages for SG1. The Δ is the difference between the inflection points of the two fitting Fermi-Dirac functions.

2020 JINST 15 C09034

2 Space resolution measurements

Space resolution in MPGD can be affected by several factors: primary statistics, electrons diffusion in gas, readout geometry, front-end electronics (digital or analog FEE) and impinging angle (θ) of the crossing particle with respect to the normal to the readout electrode (figure 11). The first four factors are usually optimized with a dedicated R&D on detector geometry, gas mixture and FEE.

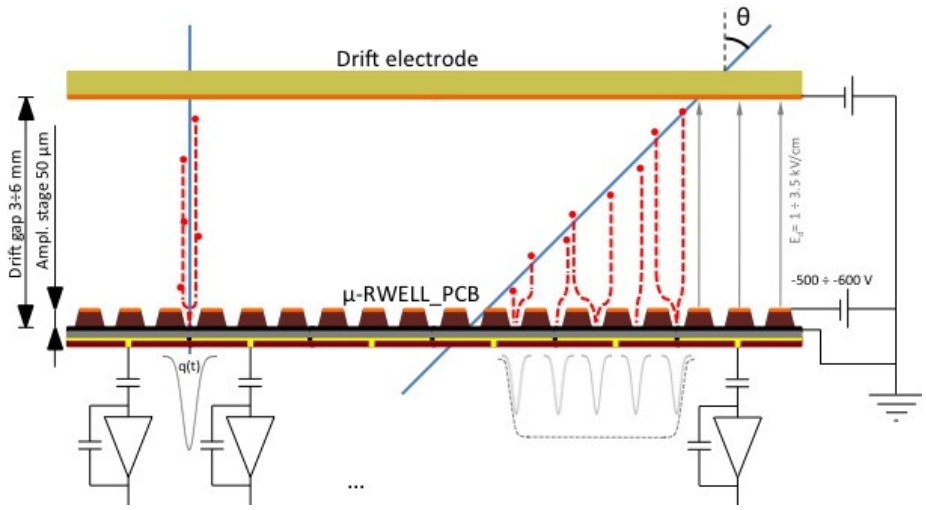

Figure 11. A simplified sketch showing how the non orthogonal tracks affect the number of fired strips.

For a detector equipped with a strip-segmented readout and instrumented with analog FEE, when a set of strips is fired the position of the track can be computed as $X_{CC} = \sum x_k q_k / \sum q_k$ where x_k is the coordinate of the k-th strip and q_k is its integrated charge. The uncertainty associated to this position is strongly dependent on the impinging angle of the track: the larger is the angle the worse is the resolution σ_x. For an experiment this means a not uniform resolution in the solid angle covered by the apparatus and results that can be consequently characterized by large systematic errors.

To overcome this issue a new algorithm has been recently proposed. The idea developed for the ATLAS MicroMegas of the New Small Wheels [10, 11], and also implemented on the BESIII cylindrical GEM [12, 13], is to reconstruct a track segment inside the detector conversion gap rather than a single hit exploiting the analog readout of the signals.

The electrons created by the ionizing particle drift towards the amplification region. By the measurement of electrons arrival time and knowing their drift velocity in the gas mixture, the position of the ionization clusters can be localized in the chamber. A fit to these clusters provide the 3D trajectory of the ionizing particle. In our case the readout is segmented in 1D strips, so only a reconstruction in what we define the $x - z$ plane is available. The fired strips represent the projection of the track on the readout and each center is the x coordinate of the corresponding ionization. These hits are recorded at different times t_k, depending on the distance of the ionization electrons from the readout plane. Applying the simple formula

$$z_k = v_{\text{drift}} \cdot (t_k - t_0) \tag{2.1}$$

the z position of the k-th cluster can be computed. The formula 2.1 exploits the good uniformity of the drift field in MPDG detectors, so that the velocity of the electrons can be considered constant. The drift velocity v_{drift} of the electrons as a function of the drift field in several gas mixtures can be found in literature. The t_0 is the common trigger time. It is crucial to define the best value for t_k. In our case, using the FEE APV25 [14], the integrated charge is sampled every 25 ns (figure 12). The leading edge of this plot is fitted with a Fermi-Dirac function and its flex point is taken as the t_k for the eq. (2.1). In figure 13 it is shown the track segment reconstruction of an event using this algorithm. The error bars on the x axis basically account for the strip pitch and for the fraction of the total charge collected on the strip (errors are increased for small charges possibly associated to charge induction); the error bars on the z axis are propagated from the time measurement uncertainty. Another possible choice for the reconstructed point errors is stated in [11].

The best position measurement corresponds to the track fit at half-gap, where the errors from the interpolation are the smallest.

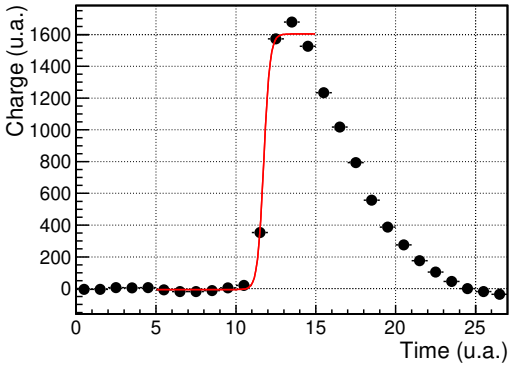

Figure 12. Integrated charge as a function of the sampling time from APV25 front end chip. The red curve is the fitting Fermi-Dirac function.

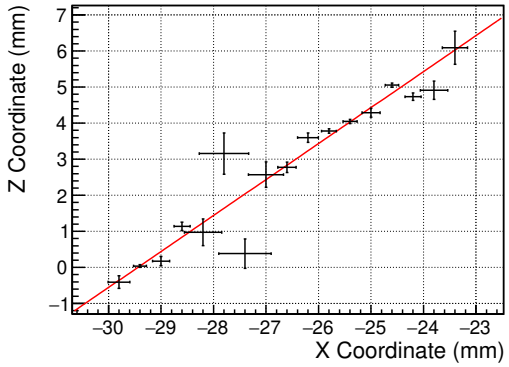

Figure 13. Example of a track segment reconstruction using the μTPC algorithm. The red line is the linear fit.

Both the CC and the μTPC algorithm has been used with μ-RWELLs during a test beam at H8-SPS CERN with a 150 GeV/c muon beam. Two μ-RWELLs have been installed on rotating plates so that the beam could form different angles with respect to the normal to the electrodes. The μ-RWELLs used in the test are derivation of the DRL layout: two metallic vias matrices connect two resistive stages to the readout plane for the grounding. The first stage is a DLC layer, while the second is made of ~ 5 mm long resistors screen-printed on a substrate. The detectors are equipped with a strip-segmented readout (400 μm pitch), operated at a gain of 5000 and readout APV25 front-end electronics and flushed with $Ar/CO_2/CF_4$ (45/15/40) gas mixture.

The space resolution can be extracted from the distribution width of the residuals (σ_{res}), that are defined as the difference between the coordinates reconstructed by the two μ-RWELLs. Indeed assuming the same contribution, the μ-RWELL space resolution is obtained as $\sigma_x = \sigma_{\text{res}}/\sqrt{2}$. For sake of simplicity in this paper all the plots showing the residual distribution are scaled by a factor of $1/\sqrt{2}$ in order to directly give the detector space resolution. The residuals are evaluated and studied for both the charge centroid and for the μTPC reconstruction.

2020 JINST 15 C09034

It is worth noticing that in an experiment it is not possible to determine which algorithm is the best since the track inclination is known just *a posteriori*, thus is required a combination of the two reconstruction methods. To estimate the effect of this combination on the global space resolution we consider the following trivial relation:

$$\frac{1}{\sigma^2_{\text{comb}}} = \frac{1}{\sigma^2_{\text{CC}}} + \frac{1}{\sigma^2_{\mu\text{TPC}}} \tag{2.2}$$

In figure 14 the resolutions for both CC and the μTPC are compared and displayed along the combined resolution from eq. (2.2). The space resolution has been evaluated at different θ using both CC and μTPC methods and the two algorithms used separately provide a not uniform space resolution. As expected for orthogonal tracks the CC provides better results while increasing the angle they quickly worsen. Vice versa the μTPC algorithm shows a better behavior for large angles than for small ones: this is reasonably correlated to the projected track segment reconstructed in the drift gap.

Since the μTPC method depends on the drift velocity of the ionization electrons in the gas mixture, and consequently on the drift field, a study at different drift fields has been performed (figure 15). For the choosen range of the electric drift field, in the used gas mixture the drift velocity of electrons is a monotonic function of the field [15]. A smaller drift velocity allows the reconstruction of the z coordinate with a smaller uncertainty, improving the μTPC fit. For orthogonal tracks the CC resolution prevails in the combination and it does not depend on the drift field in this range.

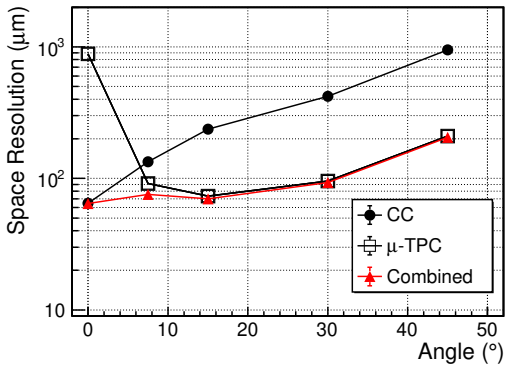

Figure 14. Comparison of the two reconstruction algorithms at a drift field E_D = 1 kV/cm.

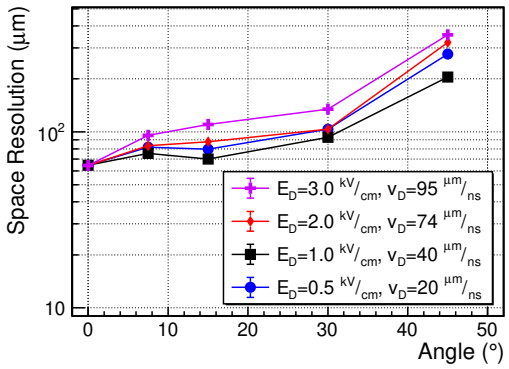

Figure 15. Combined space resolution at different drift fields with corresponding drift velocity.

2.1 Exploring the detector layout at high space resolution

For perpendicular tracks a strange pattern appears. In figures 16, 17 the X residuals as a function of the X-Y coordinates are reported. The distributions appear broader at certain values of X and Y: moreover for the figure 17 a symmetry is evident, while this does not stand for figure 16. It is worth to recall that the detectors are equipped by one-dimensional readout and thus the Y coordinate reported in figure 17 is reconstructed by external trackers. Only tracks orthogonal to the detectors have been selected.

2020 JINST 15 C09034

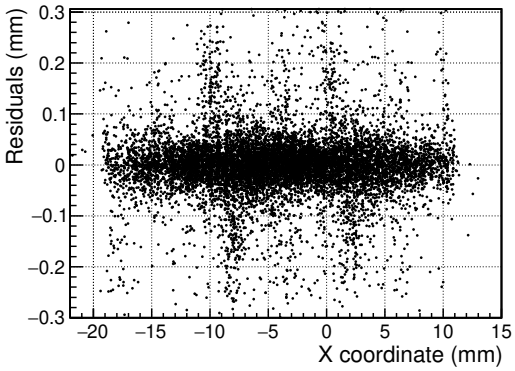

Figure 16. Residual distribution as a function of X coordinate. Perpendicular impinging particles, drift field of 3 kV/cm, CC reconstruction method.

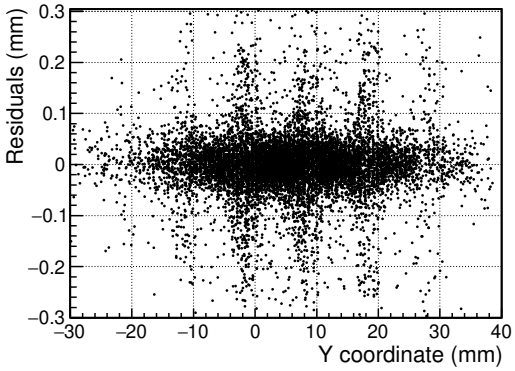

Figure 17. Residual distribution as a function of Y coordinate. Perpendicular impinging particles, drift field of 3 kV/cm, CC reconstruction method.

The bidimensional distribution of the residuals, 18, shows that the fishbone pattern follow the one of the vias of the DRL μ-RWELL. This effect appears only for perpendicular tracks, becoming quickly negligible increasing the angle, and its nature is still under investigation.

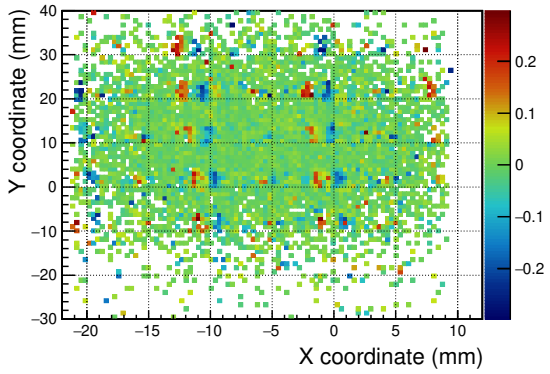

Figure 18. Residual distribution as a function of both X and Y. The distance between the yellow peaks and the blue dips is 2 mm.

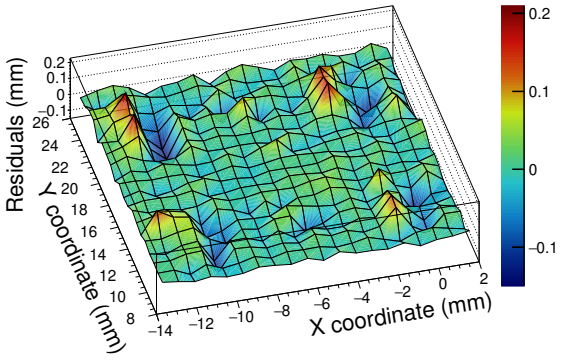

Figure 19. A $16 \times 18\,\mathrm{mm}^2$ zoom of the distribution.

3 Aging studies

A crucial point in the R&D of the μ-RWELL technology is the aging study, both for detector and DLC sheet. The demanding requirements of new HEP experiments, for example the phase 2 upgrade of the muon apparatus for LHCb experiment at LHC, suggest to verify the detector stability of operation with an integrated charge up to $1.6\,\mathrm{C/cm}^2$.

Bare DLC sheets were tested first. The easiest test is the check of the stability of the surface resistivity under normal current flow, figure 20. The DLC was connected through two concentric circular electrodes to a voltage source and the current was monitored. After $770\,\mathrm{mC/cm}^2$ the

2020 JINST 15 C09034

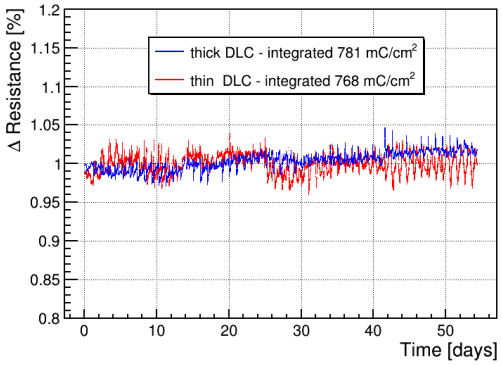

Figure 20. DLC resistance as a function of time for bare DLC.

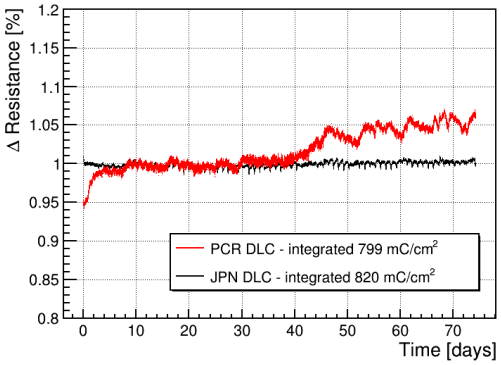

Figure 21. DLC resistance as a function of time for X-Ray irradiated DLC.

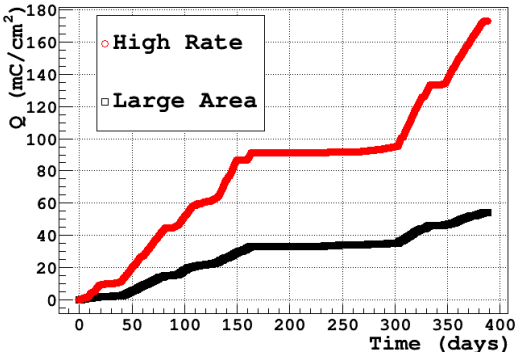

Figure 22. Charge integrated at GIF++: 175 mC/cm^2.

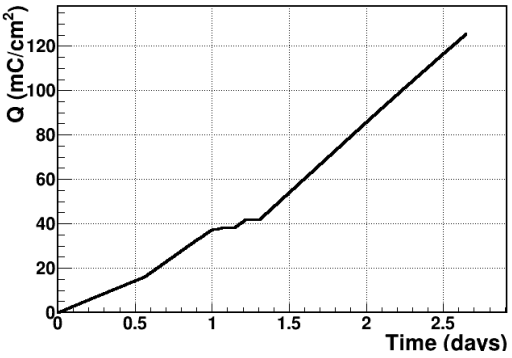

Figure 23. Charge integrated at PSI: 125 mC/cm^2.

resistance, directly related to the surface resistivity, was very stable with variations under 5%. A second test was performed with the same setup but irradiating the DLC with an X-Ray gun.[2] As the previous test, the current flow between the circular electrodes allowed to integrate 800 mC/cm^2, figure 21. The aim was to see if direct irradiation of the sheet could produce instabilites. The step of the red curve at day 40 is due to environmental effects, a minor detachment of one of the electrodes.

Preliminary results are obtained both for low rate and for high rate layouts. The exposure at GIF++ test facility at CERN integrated a charge of 180 mC/cm^2 in 250 days and in the πM1 test area at PSI each detector has integrated a charge of the order 100 mC/cm^2 (in 42 hours), figures 22 and 23, without showing any performance degradation in both the cases.

4 Conclusion

The μ-RWELL is a thin, simple and robust MPGD for very large area applications in harsh environment. The detector exhibits a gas gain up to and above 10^4 with Ar/CO_2/CF_4 (45/15/40) gas mixture. The rate capability for the high rate layouts (DRL and SG) is better than 10 MHz/cm^2

[2]X-Ray energy of 5.9 keV, 700 kHz/cm^2 on the DLC layer, with a spot of 50 cm^2.

2020 JINST 15 C09034

with a detection efficiency of the order of 97 ÷ 98%, tested with pion beam at the πM1 beam facility of the PSI. For angles lesser than 40° almost flat spatial resolution of less than 100 µm has been obtained, esploiting both the charge centroid and the µTPC algorithm, while a time resolution down to 5.7 ns has been obtained for small as well as large area detector prototypes. The aging studies, still ongoing, show promising results and no major problems, with an integrated charge of 800 mC/cm^2 with bare DLC sheets and 150 mC/cm^2 with operating detectors.

References

[1] G. Bencivenni, R. De Oliveira, G. Morello and M.P. Lener, *The micro-Resistive WELL detector: a compact spark-protected single amplification-stage MPGD*, 2015 *JINST* **10** P02008 [arXiv:1411.2466].

[2] V. Parkhomchuck, Y. Pestov and N. Petrovykh, *A spark counter with large area*, *Nucl. Instrum. Meth.* **93** (1971) 269.

[3] M. Anelli, G. Bencivenni, G. Felici and L. Magro, *Glass electrode spark counters*, *Nucl. Instrum. Meth. A* **300** (1991) 572.

[4] G. Bencivenni, R. De Oliveira, G. Felici, M. Gatta, M. Giovannetti, G. Morello et al., *The µ-RWELL layouts for high particle rate*, 2019 *JINST* **14** P05014 [arXiv:1903.11017].

[5] G. Bencivenni et al., *The µ-RWELL detector*, 2017 *JINST* **12** C06027.

[6] G. Bencivenni, R. De Oliveira, G. Felici, M. Gatta, G. Morello, A. Ochi et al., *Performance of µ-RWELL detector vs resistivity of the resistive stage*, *Nucl. Instrum. Meth. A* **886** (2018) 36.

[7] G. Bencivenni, G. Felici, F. Murtas, P. Valente, W. Bonivento, A. Cardini et al., *A triple GEM detector with pad readout for high rate charged particle triggering*, *Nucl. Instrum. Meth. A* **488** (2002) 493.

[8] C. Richter, A. Breskin, R. Chechik, G. Garty and A. Sharma, *Absolute electron transfer efficiency of GEM*, *Nucl. Instrum. Meth. A* **461** (2001) 38.

[9] A. Balla, G. Bencivenni, P. Branchini, P. Ciambrone, E. Czerwinski, E. De Lucia et al., *The KLOE-2 Inner Tracker: Detector commissioning and operation*, *Nucl. Instrum. Meth. A* **845** (2017) 266.

[10] T. Alexopoulos, J. Burnens, R. de Oliveira, G. Glonti, O. Pizzirusso, V. Polychronakos et al., *A spark-resistant bulk-MicrOMEGAs chamber for high-rate applications*, *Nucl. Instrum. Meth. A* **640** (2011) 110.

[11] T. Alexopoulos et al., *Performance studies of resistive-strip bulk MicrOMEGAs detectors in view of the ATLAS New Small Wheel upgrade*, *Nucl. Instrum. Meth. A* **937** (2019) 125.

[12] L. Lavezzi et al., *Performance of the micro-TPC Reconstruction for GEM Detectors at High Rate*, in proceedings of *IEEE Nuclear Science Symposium and Medical Imaging Conference*, Atlanta, GA, U.S.A., 21–28 October 2017, pp. 1–5 [arXiv:1803.07266].

[13] S. Marcello et al., *The new CGEM Inner Tracker and the new TIGER ASIC for the BES III Experiment*, *PoS* **EPS-HEP2017** (2017) 505.

[14] M. Raymond et al., *The APV25 0.25 µm CMOS readout chip for the CMS tracker*, *IEEE Nucl. Sci. Symp. Conf. Rec.* **2** (2000) 9/113.

[15] M. Alfonsi, G. Bencivenni, P. De Simone, F. Murtas, M. Poli-Lener, W. Bonivento et al., *High-rate particle triggering with triple-GEM detector*, *Nucl. Instrum. Meth. A* **518** (2004) 106.

2020 JINST 15 C09034